ISABE-2011-1129

EXPERIMENTAL RESULTS SHOWING THE INTERNAL THREE-COMPONENT VELOCITY FIELD AND OUTLET TEMPERATURE CONTOURS FOR A MODEL GAS TURBINE COMBUSTOR

BC Meyers*, GC Snedden**, JP Meyer*, TH Roos**, GI Mahmood*
*University of Pretoria, Department of Mechanical and Aeronautical Engineering, Pretoria, South Africa
**CSIR, DPSS, PO Box 395, Pretoria, 0001, South Africa
bmeyers@csir.co.za (BC Meyers)

Abstract

A three-component flow field inside a can-type, forward flow experimental combustor was measured under non-reacting conditions. The combustor was run at atmospheric conditions with the air flow supplied from a fan and the outlet was straight to atmosphere. Temperature data, under reacting conditions, in the combustor was also obtained using a thermocouple rake as well as an outlet velocity profile using a Pitot tube at reacting and non-reacting conditions.

For the flowfield measurements a stereoscopic PIV system was used to measure the flow field data thus an optically accessible combustor was required. The combustor for these experiments was manufactured out of Perspex and thus only non-reacting experiments could be performed. This combustor was a replica of the metal combustor used for the reacting experiments except for the slightly thicker walls.

Nomenclature

Symbols

*	Position markers
α	Angle of rake rotation
Δp	Pressure difference
Φ	Diameter
$\dot{m}$	Flow rate
p	Static pressure
T	Temperature
U	Axial velocity
V	Radial velocity
W	Azimuthal velocity

Abbreviations

4M	4 Megapixel
AFR	Air/Fuel ratio
CCD	Charged couple device
CFD	Computational fluid dynamics
ID	Inner diameter
LDV	Laser doppler velocimetry
Mag	Magnitude
PIV	Particle image velocimetry
Vel	Velocity

Subscripts

1	Fan outlet
3	Combustor inlet
4	Combustor outlet
A	Air
a	Position identifier
AFT	Adiabatic flame temperature
atm	Atmospheric
b	Position identifier
c	Position identifier
F	Fuel
i	Index
L	(Combustor) Liner
OP	Orifice plate

Introduction

There are often inconsistencies when comparing experimental and Computational Fluid Dynamics (CFD) simulations for gas turbine combustors [1,2]. These inconsistencies are especially great when combustion is simulated when there are already flow inconsistencies after modeling the flow in cold flow simulations. To enable the improvement of CFD modeling and techniques, a CFD test case has been created to aid in simulation validation and improvement.

The study provides a collection of experimental data for the validation of CFD results. The validation step is to create a mechanism to tailor the CFD method to model the combustor as correctly as possible. This allows for CFD to be used as a reliable design tool for gas turbine combustor whether it is for the proving of a combustor design concept or the optimization of a preliminary design [2,3,4].

The method of simulating gas turbine combustors usually involves a cold flow simulation first to ensure that the flow phenomena are captured correctly [1,3].

The combustion modeling is dependent on the flow modeling and thus this part is added to the simulation after the flow is captured satisfactorily [2,5]. For the validation of the cold flow simulations, the velocity field in a generic can-type gas turbine combustor, running at atmospheric conditions, was measured in using a stereoscopic Particle Image Velocimetry (PIV) system. Once the non-reacting flow has been modeled satisfactorily the reacting flow can then be modeled. For the validation of this stage of the simulation process, the outlet plane temperature profile was measured with a thermocouple rake rotated 360° at the outlet. The outlet velocity profile both with and without combustion was also measured.

Previous data presented for this particular combustor was for cold flow (non-reacting) runs at 60% of the design mass flow rate [6]. This paper will include both velocity and temperature data captured close to (90%) the design air mass flow rate for this experimental combustor of 0.1 kg/s. Similar to Carl et al. [7], attempts have to be made to ensure that as many of the factors that influence the combustor flow should be included in the tests. The combustor in which these experiments were performed is a full, non-premixed, cylindrical, can-type combustor which includes an injector at the centre of a swirler in the dome of the combustor. The combustor has all three typical combustor zones i.e. a primary zone, secondary zone and dilution zone all with their respective holes. Two sets of cooling rings with holes are also included before and after the secondary zone.

Experimental Setup

Test Rig

The experimental rig is the same as that used in the experiments presented by Meyers et al. [6] in 2009. Figure 1 shows a schematic diagram of the test rig. The air for combustion is supplied by a fan run by an 11 kW motor. The fan air exits into a set of pipes, which house an orifice plate and allow the flow to develop, with the combustor liner placed at the end of the pipes at the outlet. The combustor then exhausts to atmosphere through a short exhaust/outlet pipe.

The combustor liner is a non-premixed generic can-type combustor which has a single swirler in the upstream dome end. A metal combustor liner and casing was used to collect the temperature and velocity profiles under reacting conditions. While a Perspex combustor liner and casing were used to capture the more detailed velocity field data inside the combustor liner using the PIV technique. The Perspex and metal test sections were interchangeable. The transparent combustor was manufactured such that the combustor liner inner diameters and holes were identical to the metal combustor. Due to the slightly thicker walls of the Perspex liner, the outer diameter was not the same as the metal liner thus the annulus hydraulic diameter was matched making the Perspex casing ID = 121.2 mm. Details of the Perspex liner can be found in Meyers et al. [6].

The reacting experiments were performed using the metal test section with the stainless steel 304 combustor liner which is shown in Figure 2 and Figure 3. The dimensions shown in red indicate those that varied from the Perspex liner. Figure 4 shows the five K-Type thermocouple rake that was rotated around the rail to get a full outlet plane contour plot of the outlet temperature profile. Figure 5 shows the velocity profiles at the exhaust being measured using a Pitot tube.

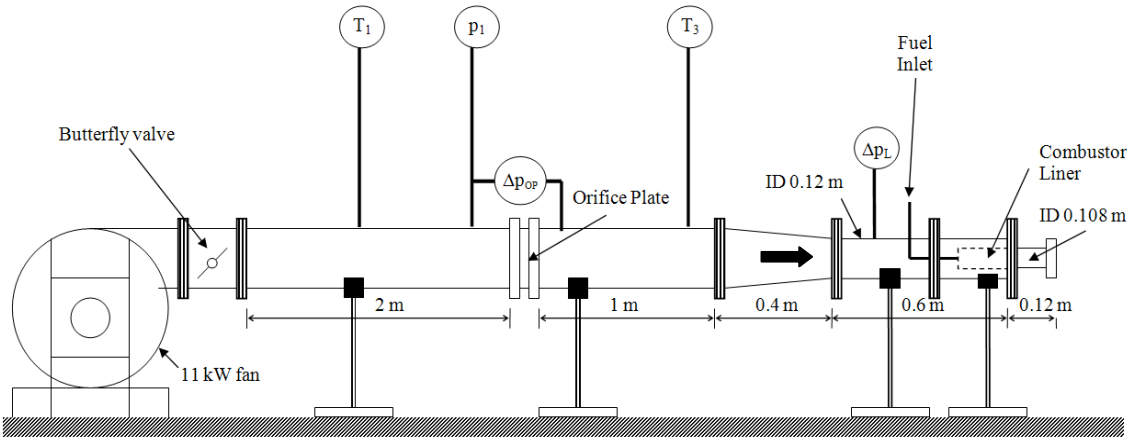

Figure 1: A schematic diagram of the test rig.

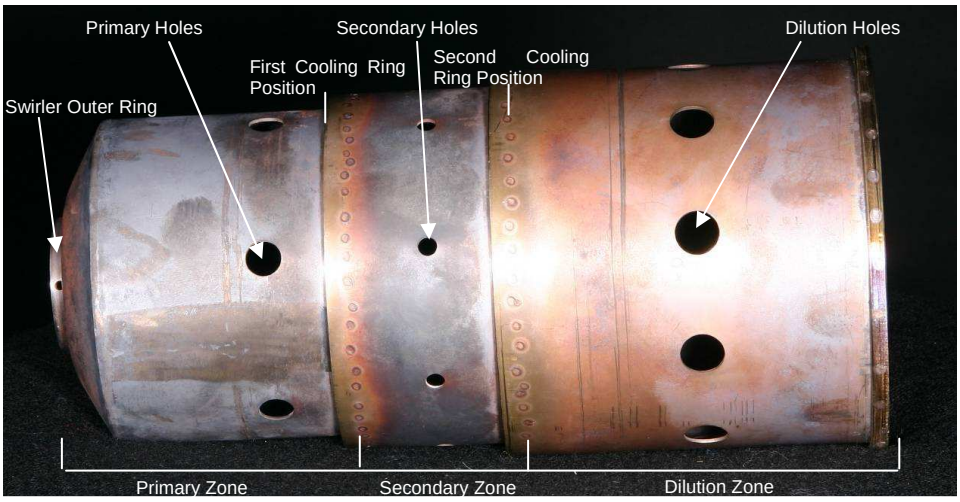

Figure 2: The stainless steel combustor liner used for reacting experiments.

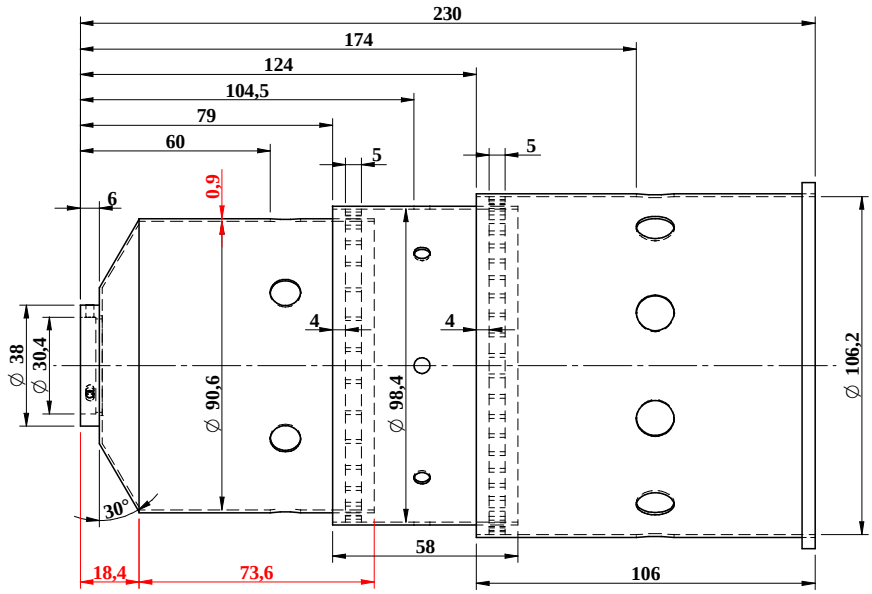

Figure 3: A detailed drawing of the Metal combustor. Red dimensions vary between the metal and Perspex combustors.

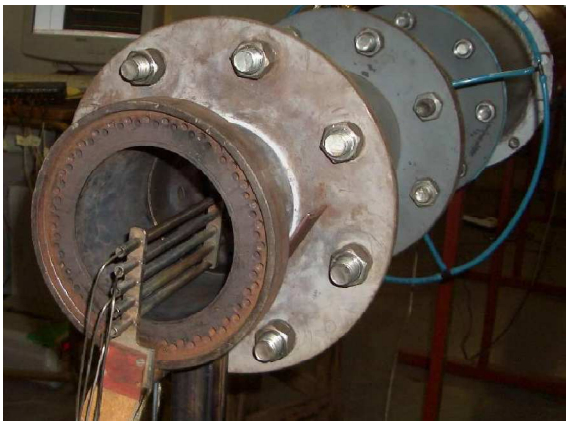

Figure 4: The five K-type thermocouples in a rake at the combustor outlet.

Figure 5: A magnetic clamp holds the Pitot tube onto the test rig in the correct position.

Test Conditions

All experiments were performed at the similar altitudes thus resulting in an average atmospheric pressure of 86.1 kPa. The average inlet temperature was 327.4 K for the non-reacting tests and 307.1 K for the reacting tests.

For the PIV experiments, each of the three zones of the combustor were tested separately with the laser sheet in line and in between the respective holes. Three-component velocity vectors were obtained throughout the combustor. For each experiment the top camera was at 5° and the bottom camera at 20° to the normal of the laser sheet. The data presented here is for an air mass flow rate of 0.089 kg/s (320 kg/h).

In order to perform the temperature measurements, the thermocouple rake was rotated in order to measure the temperatures at five points per position at 10° intervals. The tips of the thermocouples were aligned at the outlet plane of the combustor liner. The mass flow during these experiments was 0.090 kg/s (326 kg/h).

The velocity profiles were measured at the outlet to the test rig exhaust using a Pitot tube. The Pitot tube was moved in 5 mm increments along the horizontal diameter of the exhaust pipe. The velocity profile was measured in reacting and non-reacting conditions at a mass flow rate of 0.092 kg/s (331 kg/h).

The average mass flow rate for all of the presented experiments was 0.09 kg/s. For the reacting experiments, the fuel flow rate, $\dot{m}_F$, was 0.784 g/s giving an average AFR of 114.7. The nozzle used produced a cone shaped spray with a 40° half angle. The fuel used was Kerosene.

Instrumentation

A TSI stereoscopic PIV system was used for velocity field measurements. It has a dual laser head enabling a minimum of 1 µs pulse separation time between laser flashes. The laser heads are Big Sky Laser CFR 200s attached to frequency doubling and alignment optics. These optics enable both laser heads to emit a beam through the same outlet and to convert the 1064 nm wavelength to a 532 nm wavelength. The laser beam is then passed into a laser arm which places the light in the required position. A -25 mm focal point cylindrical lens turns the beam into a sheet and a 500 mm focal point spherical lens focuses the sheet to give it a sheet thickness of approximately 1.5 mm in the test section. The laser sheet was aligned with the axial flow direction of the combustor liner.

The flow was seeded using smoke produced from burning oil. The cameras were required to be approximately 200 mm away from the combustor. This distance was chosen firstly to fill as much of the camera frame with the region of interest in the combustor as possible, and secondly because the smoke particles did not reflect light with enough intensity to place the cameras much further away.

The two cameras used were Powerview 4M Plus greyscale CCD cameras each with a 2048 x 2048 pixel array. These cameras were attached to a rail facing the test section with the Sheimflüg angle satisfied for PIV data collection. Both cameras were on the same side of the laser sheet with the top camera in back scatter and the bottom camera in forward scatter.

For each experiment 720 three-dimensional vector fields were averaged to get a steady state vector field. The TSI software Insight3G [8] was used to analyse the images captured and Tecplot [9] was used to average the data.

The thermocouples used for the temperature contour measurements were K-Type thermocouples in 2 mm diameter stainless steel sheaths from WIKA Instruments. These were placed manually into the rake which was constructed to provide a more precise positioning of the thermocouples as well as some radiation shielding from the lateral directions to the thermocouples. The thermocouples were connected to an IOTech personal Daq 3000 Series data acquisition system.

The Pitot tube used had a 90° bend in it to enable the manometer to be connected to the tube at a location that is out of direct contact with the exhaust gasses. The manometer used was a dpm t-series digital manometer.

Uncertainty

Table 1 lists the uncertainties of the results and inputs presented. Different methods were used for the various uncertainty calculations.

Li and Gutmark [5] have stated that the uncertainty of PIV is greater than that of LDV which is taken as ±5% and thus was assumed to be of the order of ±5-10%. The PIV system was validated against a Pitot tube measurement of the axial component in a specially designed experiment. At the core of the flow the pitot tube and the PIV profile lie reasonably close with the pitot tube lying within the PIV scatter band which has an average of 3.2% in this region and the profiles followed a similar trend even at the edges of the flow.

The uncertainty of the thermocouple readings was determined by calibration and using the Standard Error of Estimate for the uncertainty calculation. The rest of the uncertainties were calculated using the Kline-McClintock method [10]. Note that to measure

the atmospheric pressure, p_{atm}, a Fortin barometer was used for the reacting experiments and a Kews barometer for the PIV experiments.

Table 1: The uncertainties of the various results shown.

Variable	Instrument	Units	Uncertainty
p_{atm}	Fortin Barometer	Pa	± 30.2
	Kews barometer	Pa	± 17.3
T_3	K-type	K	± 1.1
$\dot{m}_A$	Orifice Plate	kg/s	± 1.01%
$\dot{m}_F$	Calculated	kg/s	± 6.7 x 10^{-6}
AFR	Calculated	-	± 1.32
U, V, W	PIV	m/s	± 3.2-10%
U	Pitot Tube	m/s	± 1.05%
T_4	K-type	K	± 3.4
Pattern factor	Calculated	-	± 0.0068
Profile factor	Calculated	-	± 0.0017
Overall pressure loss	Calculated	%	± 1.97%
Pressure loss factor	Calculated	-	± 2.15%

Experimental Results

The velocity data was collected on a plane lying lengthwise along the central axis. This plane was chosen because it would encompass a large amount of information and it was one of the few orientations that would allow the cameras to be positioned such that large areas could be measured. The data on this plane is shown to be close to symmetrical throughout the length of the combustor.

Velocity Fields

In line with holes

The velocity magnitude contours and streamlines are shown in a normal view of the combustor liner in Figure 6. This plane is aligned with the holes of all three zones. Streamlines are superimposed over the contour plot in order to highlight the main flow features.

The main features shown in these figures include the inlet flow in the diffuser before the combustor liner, the recirculation zone in the primary zone showing the mechanism for flame stabilisation, the jet velocities and penetration depths for all three of the zones (primary, secondary and dilution) as well as an unexpected recirculation region in the dilution zone.

In Figure 6a, the bulk flow in the diffuser can be seen at (1). The velocities here are slow relative to the velocities within the combustor liner.

Within the primary zone, the flame stabilizing features of reverse flow (2) and a swirling recirculation zone (3) can be seen. The reverse flow region is quite a rectangular shape and does not have the characteristic cone- or Y-shape [11].

The stagnation point at (4) occurs due to the jets at (5) having a 100% penetration depth. The penetration depth in this instance is determined by the radial distance from the wall, as a percentage of the radius, at which the streamlines from the jets become asymptotic to the main combustor flow.

In the secondary zone, some flow in the annulus is evident at (6), while the continuation of the forward flow out of the primary zone is evident at (7). In this region the stream lines tend to diverge towards the liner wall until the secondary jets are encountered at (8). The secondary jets penetrate about 60% into the main combustor flow. After the jets the streamlines diverge again.

The divergent flow in the secondary zone feeds into the outer region of a recirculation zone in the dilution zone (9). Along with the recirculation zone a reverse flow region is formed in the centre and is shown at (10). The dilution zone jets (11) also have a 100% penetration and they impinge on each other at the centre. After the jets a forward flow region is set up where the flow then exits the combustor liner (12). Empirical calculations show that these jets receive 50% if the total mass flow thus explaining the 100% penetration depth. Similarly, the primary jets receive 22.5% of the total mass flow. The dilution hole set, however, has a large number of large diameter holes so the velocity of the jet decreases at a faster rate than the primary jets.

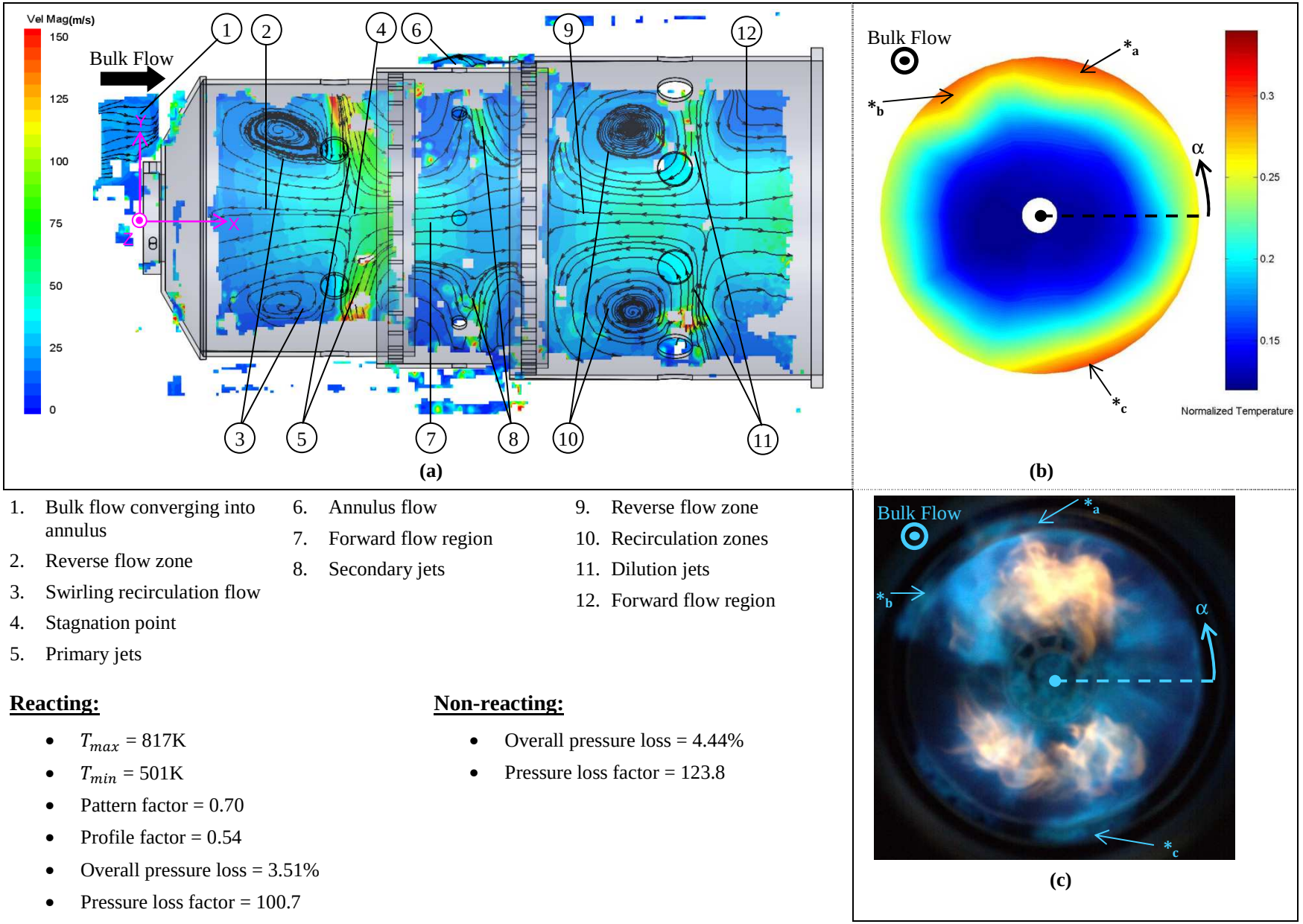

1. Bulk flow converging into annulus
2. Reverse flow zone
3. Swirling recirculation flow
4. Stagnation point
5. Primary jets
6. Annulus flow
7. Forward flow region
8. Secondary jets
9. Reverse flow zone
10. Recirculation zones
11. Dilution jets
12. Forward flow region

Reacting:

- T_{max} = 817K
- T_{min} = 501K
- Pattern factor = 0.70
- Profile factor = 0.54
- Overall pressure loss = 3.51%
- Pressure loss factor = 100.7

Non-reacting:

- Overall pressure loss = 4.44%
- Pressure loss factor = 123.8

Figure 6: In line with the holes at $\dot{m}_A$ = 0.09 kg/s: (a) A contour plot of velocity magnitude along with streamlines (non-reacting) (b) A normalised temperature contour plot on the outlet plane of the combustor liner (reacting) and (c) a photograph of the flames during a reacting run.

The secondary zone jets only receives 8.8% of the total mass flow hence the decreased penetration depths of 60%. There is also no change in the penetration depths due to the increase in the total mass flow of this study.

In a previous study the data collected at a lower mass flow rate [6] shows more of the subtle features which are not evident in the current data. This is due to the increased velocities which make capturing data more difficult, particularly in the out of plane Z direction. The features that are missing in this data set are: 1) the bulk flow splitting off to enter the swirler, 2) the annulus flow curving into a primary zone hole to form a jet; 3) annulus flow converging into a smaller annulus around the successive zones

In between holes

Due to the lower velocities in between the holes, a larger delay between laser pulses would be possible. This improves the ability to collect data, thus some of the more subtle features can be observed in the vector field such as the convergence of the bulk flow to enter the annulus around the combustor liner at (13).

In Figure 7 the planes are in between the holes of each of the respective zones. The primary zone plane is at 30° to the plane in line with the holes, the secondary zone is at 22.5° and the dilution zone is at 18°. All three planes are viewed normally. In this figure the velocity magnitude contours are shown with the streamlines superimposed.

The flow structures in the primary zone are similar to those shown in line with the holes. There is a reverse flow region (14), a recirculation zone (15) and even streamlines converging at the centreline (16) as in line with the holes where the jets are present.

The secondary zone has the most significant difference due to the lack of jets showing a constant divergence (17) of the streamlines throughout the length of the zone. The rest of the zone, however, remains unchanged.

As in the previous two zones, in the dilution zone there are many of the same features in between the holes as in line with the holes. These include: the reverse flow region (18), the recirculation zone (19) and the converging streamlines at the position where the jets are in line with the holes. A main difference though is present on the outer edges of the two recirculation zones in this section. The outer side of the recirculation zone leaves the vortex structure and flows along the wall to join the bulk flow of the combustor at (21). In the plane in line with the holes, however, the recirculating flow is blocked by the jets and remains in the recirculating zone.

Velocity Profiles

Figure 8 to Figure 10 and Figure 12 to Figure 14 show the velocity profiles extracted from the velocity fields (Figure 6 and Figure 7) at various axial positions in the combustor liner for ease of data interpretation. The positive and negative values of the profiles are shown with the X, Y and Z axes shown at X=0 mm. On the azimuthal profiles, a negative value indicates the flow would be going into the page and a positive value out of the page.

In line with holes

Figure 8, Figure 9 and Figure 10 show the axial (U), radial (V) and azimuthal (W) velocity profiles in line with the holes, respectively.

In Figure 8, the bulk flow is shown before the combustor liner in Profile A and B. Profile A has a maximum axial velocity of 18 m/s. The velocity Profiles D to F at X = 29, 48 and 61 mm show the profile shapes in the recirculation zone with a negative value in the core of the combustor and a positive value around the edge of the combustor flow. After these the last two primary zone profiles, G and H show a transition into a positive/forward flow profile with the maximum axial velocity on H at 55 m/s.

In the secondary zone the axial velocity has a decreasing trend in magnitude due to the transition into the reverse flow and recirculation zones of the dilution zone.

In the dilution zone as in the primary zone, the recirculation zone with a negative value in the core of the combustor and a positive value around the edge of the combustor can be seen in Profiles M to R. The maximum negative velocity in the dilution zone of 40 m/s is in the core on Profile O. The outlet velocity profile has the maximum positive velocity of 44 m/s (Profile U) with the outer edges of the profile close to 0 m/s.

The radial velocity profiles are shown in Figure 9a & b. The profiles that go through the jets are separated out into Figure 9b for clarity. The maximum jet velocity shown is in the primary zone showing 95 m/s on Profile G. The maximum radial velocity in the jets, from the velocity contours is, however, of the order of 110 m/s. the maximum velocity on Profile K is 60 m/s and the maximum velocity on Profile R is 58 m/s.

Figure 10 shows the azimuthal velocity profiles in line with the holes. Profiles A to C, G and H have been removed to make the figure clearer. In all of the profiles shown, at least near the centre, it is evident that the velocities above the centre line are to the negative direction and in the positive direction below the centre line.

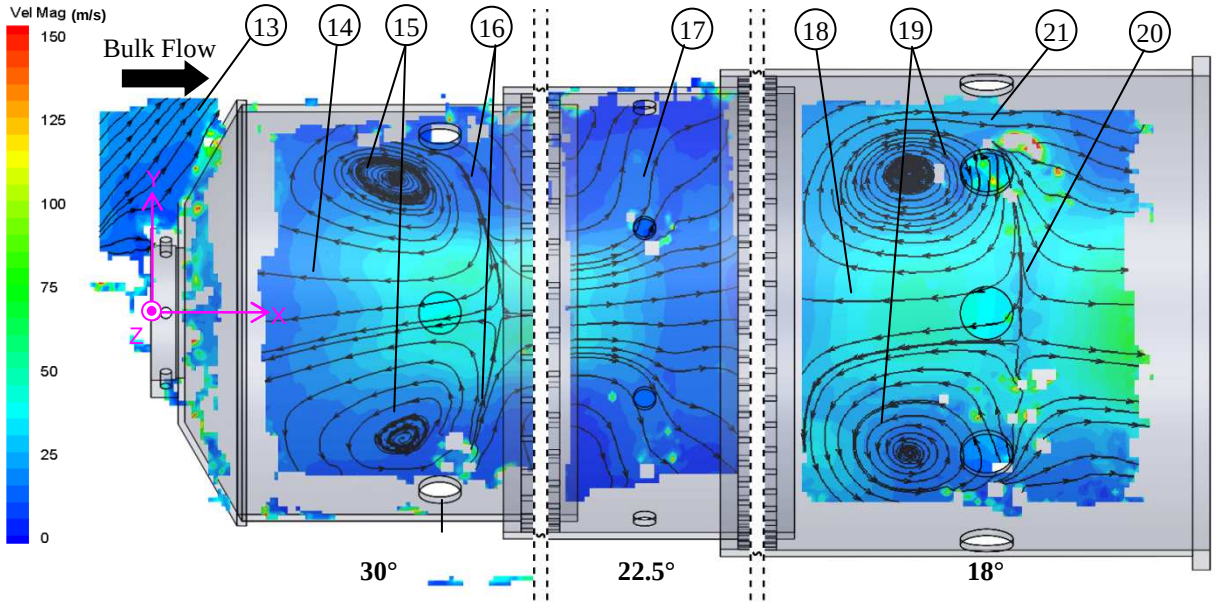

Figure 7: In between with the holes at $\dot{m}_A$ = 0.09 kg/s: A contour plot of velocity magnitude along with streamlines (non-reacting).

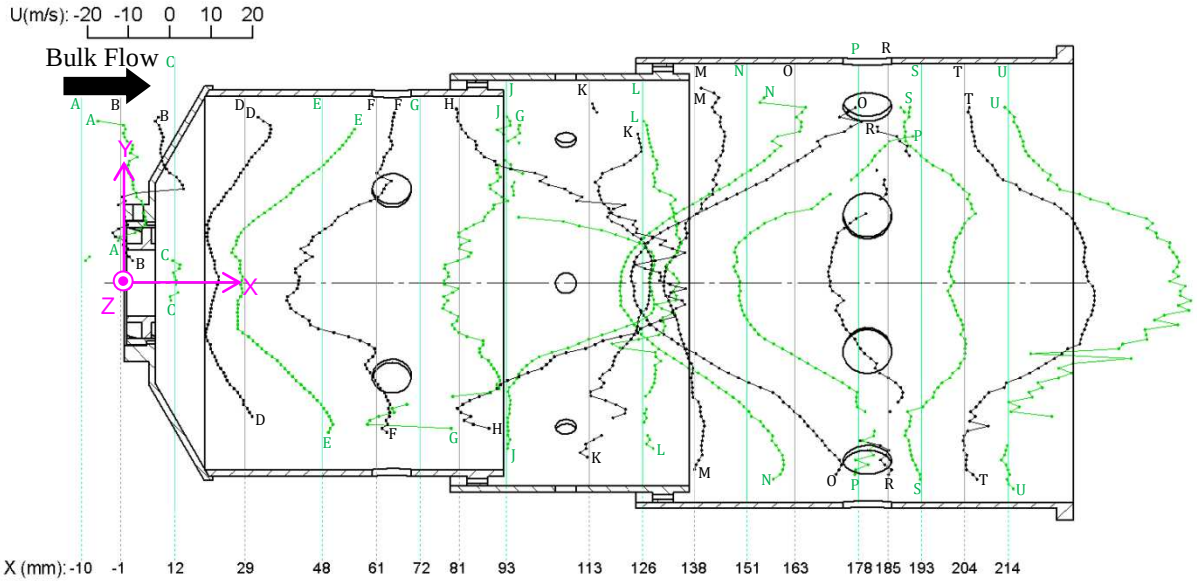

Figure 8: In line with the holes at $\dot{m}_A$ = 0.09 kg/s: The axial velocity profiles at various positions of the respective zones.

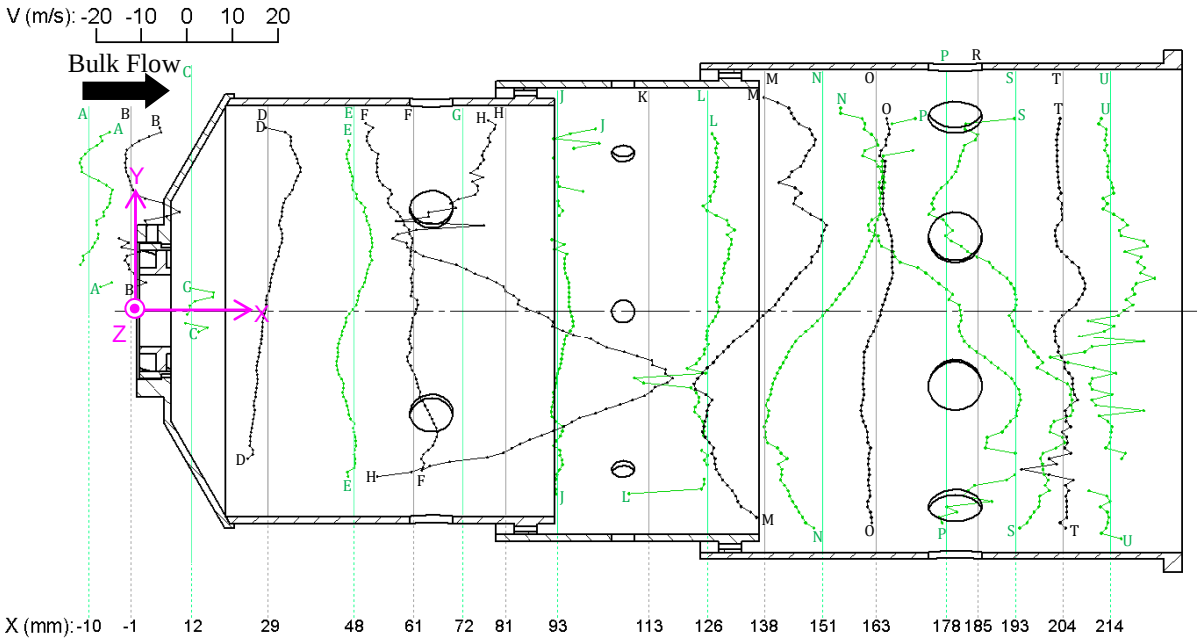

(a)

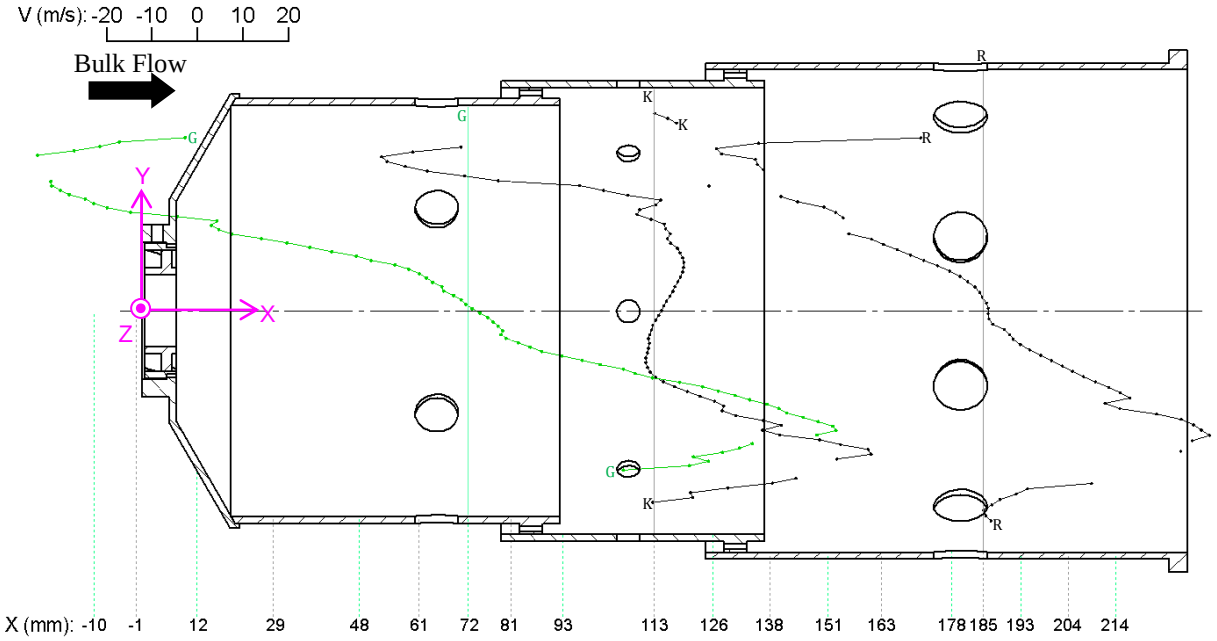

(b)

Figure 9: In line with the holes at $\dot{m}_A$ = 0.09 kg/s: The radial velocity profiles at various positions of the respective zones with (a) no jet profiles and (b) jet profiles only.

These profiles show the swirling motion introduced by the swirler. When studying the profiles more closely, a trend is shown that the swirl velocity decreases as one moves away from the centre towards the liner wall. This is especially evident in the primary zone Profiles D, E and F. In these profiles, the maximum velocity magnitudes are 8.8, 12.8 and 34 m/s respectively.

In the secondary zone, near the centerline, the swirl is shown to be less intense than in the primary zone. In the dilution zone, however, there is a slight increase in the swirl intensity especially near the centre. Near the wall however the swirl seems to all but disappear.

In between the holes

Data collected in between the holes is discussed in this section. The planes on which the data was collected in each of the three combustor zones as well as the plane on which the Pitot tube data was collected in the outlet pipe are shown in Figure 11.

Figure 12 to Figure 14 show the velocity profiles extracted from the PIV velocity fields in between the holes. The axial velocities are shown in Figure 12. The shapes of the velocity profiles at the various positions are similar to those shown in Figure 8, however, due to there not being jets present, the profiles tend to be smoother. In the bulk flow region on Profile A, a maximum axial velocity of 6.4 m/s is shown. Profile G in this plane has a negative value near the centre as opposed to a positive value that is seen in line with the holes in Figure 8.

The secondary zone again shows a decreasing trend in the axial velocity magnitudes especially near the centreline.

In the dilution zone, the liner outlet velocity profile (Profile U) has a maximum velocity of 63.5 m/s.

The velocity profiles measured using a Pitot tube were measured both during combustion (reacting) and without combustion (non-reacting) on the metal combustor. These two velocity profiles are shown in Figure 12 in red for the reacting/hot case and blue for the non-reacting/cold case. The maximum velocity with combustion (44.5 m/s) is almost twice that without combustion (26.5 m/s). The average velocities also show this trend with the average velocity without combustion at 9.8 m/s and 20.1 m/s with combustion.

Figure 13 shows the radial velocities throughout the combustor liner. The profiles are all very similar to those shown in line with the holes except, as expected, where the jets were on profiles G, K and R. Profile K shows the diverging trend that was described above in the secondary zone when the jets are not present.

For the azimuthal velocities shown in Figure 14, the secondary and dilution zones also have similar shapes and magnitudes to those in line with the holes in Figure 10. In the primary zone, however, there seems to be an increase in the swirl intensity especially at the profiles just before (Profile F). Profile D, E and F have maximum velocities of 13, 16 and 22.5 m/s respectively.

Temperature contours

The temperatures measured using the thermocouple rake were normalized to compensate for the variation in atmospheric temperature and the fuel used. This was done using the following equation:

$$Normalised\ Temperature = \frac{T_{4i} - \overline{T_3}}{\overline{T_{AFT}} - \overline{T_3}}$$

The contour map of the normalized temperatures is shown in Figure 6b. The contour map was measured at the outlet plane to the combustor liner.

The measurements show that the outlet temperature profile was not as symmetrical as expected from the symmetrical geometry. There were hot regions from about 45° to 135° and from about 260° to 340°[1]. The cold region pushed from the centre through to the walls in between the hot spots. There was also an undulation in the hot region in the 45° to 135° sector.

The reason for the hot outer edge and the cold core is evident when one looks at the path that the hot flow would follow in the planes in between the holes. It can be seen in Figure 7 that the hot combustion gasses would leave the primary zone along the outer edge of the recirculation zone to move on to the secondary zone along the wall. The divergent trend in the secondary zone would keep the hot gasses towards the liner wall. The hot gasses would then get entrained into the dilution zone recirculation zone and again be forced towards the outer edge of the combustor liner. The hot gasses (mixed with some of the cooler dilution air) then leaves the recirculation zone along the wall at (21) in Figure 7.

Further reinforcement of the cold core occurs on the planes in line with the holes where the primary and especially the dilution jets have 100% penetration allowing the coldest air to be injected at the centreline and to then travel downstream at the core.

[1] α is measured from the dashed horizontal line shown in Figure 6 in an anti-clockwise direction for all angle references for the temperature measurements.

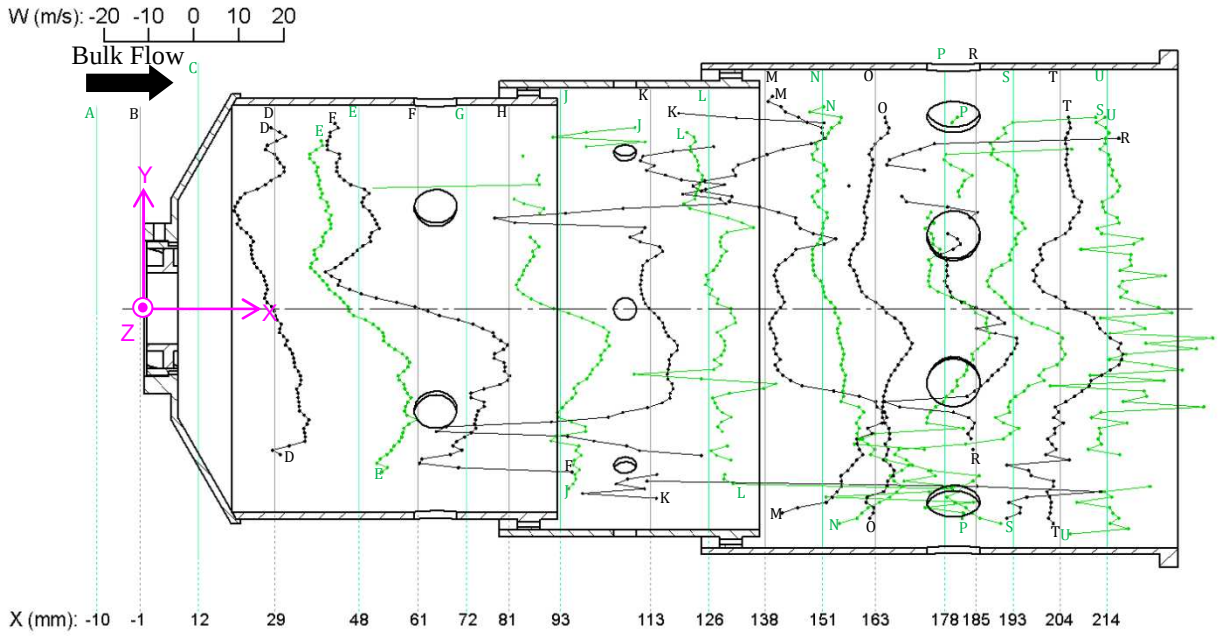

Figure 10: In line with the holes at $\dot{m}_A$ = 0.09 kg/s: The azimuthal velocity profiles at various positions of the respective zones.

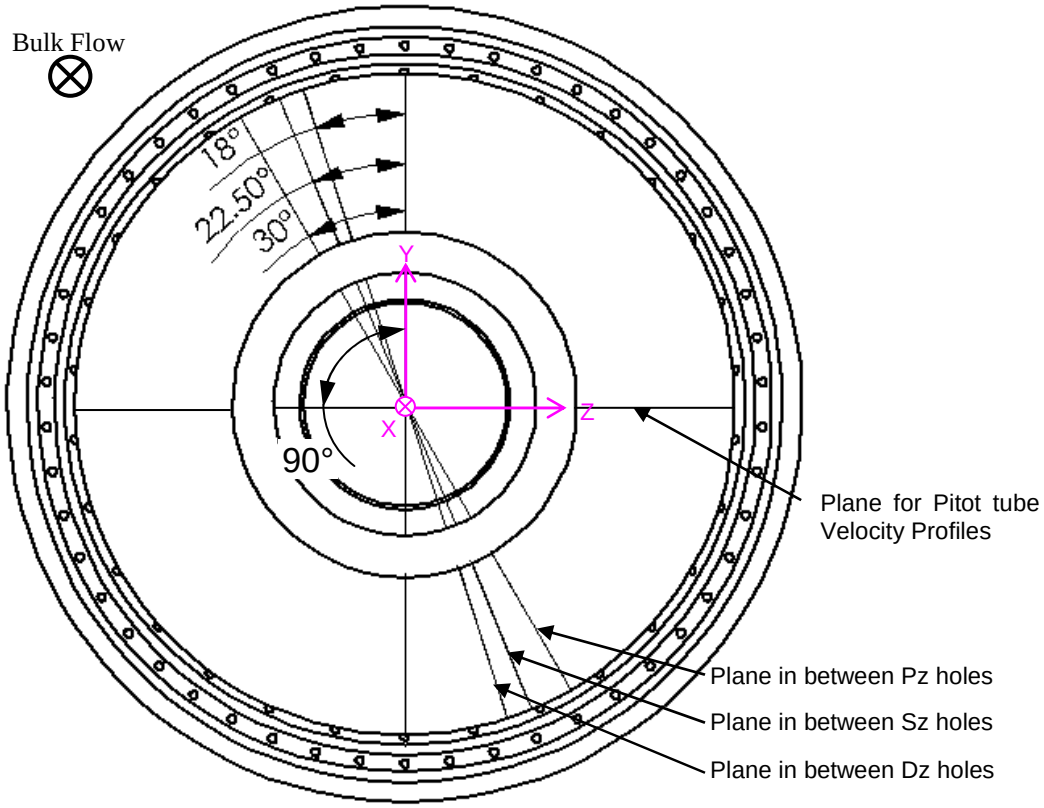

Figure 11: The angles showing the positions of the planes in between the holes and the pitot tube velocity plane.

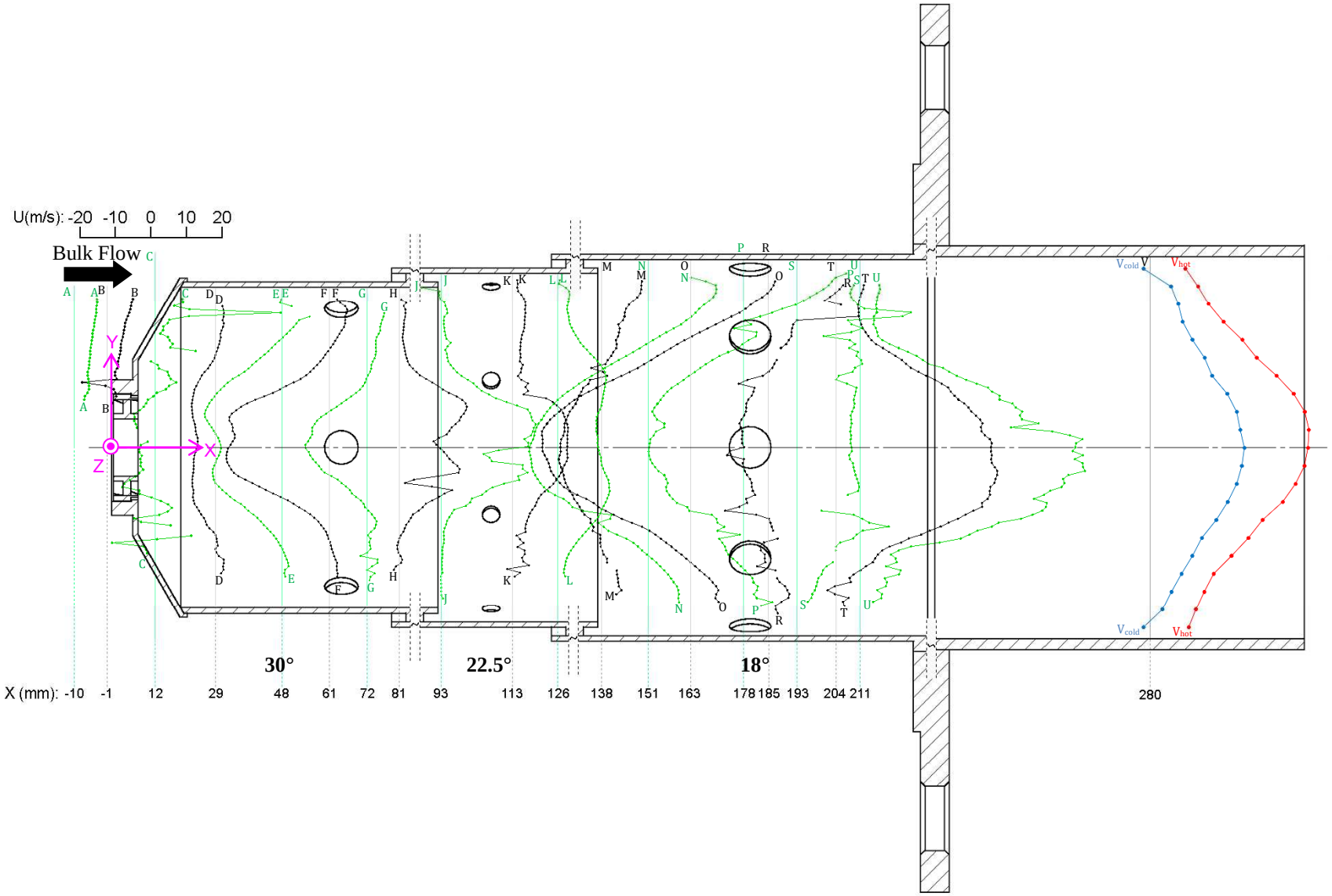

Figure 12: In between with the holes at $\dot{m}_A$ = 0.09 kg/s: The axial velocity profiles at various positions of the respective zones as well as the Pitot tube velocity profiles in the exhaust pipe.

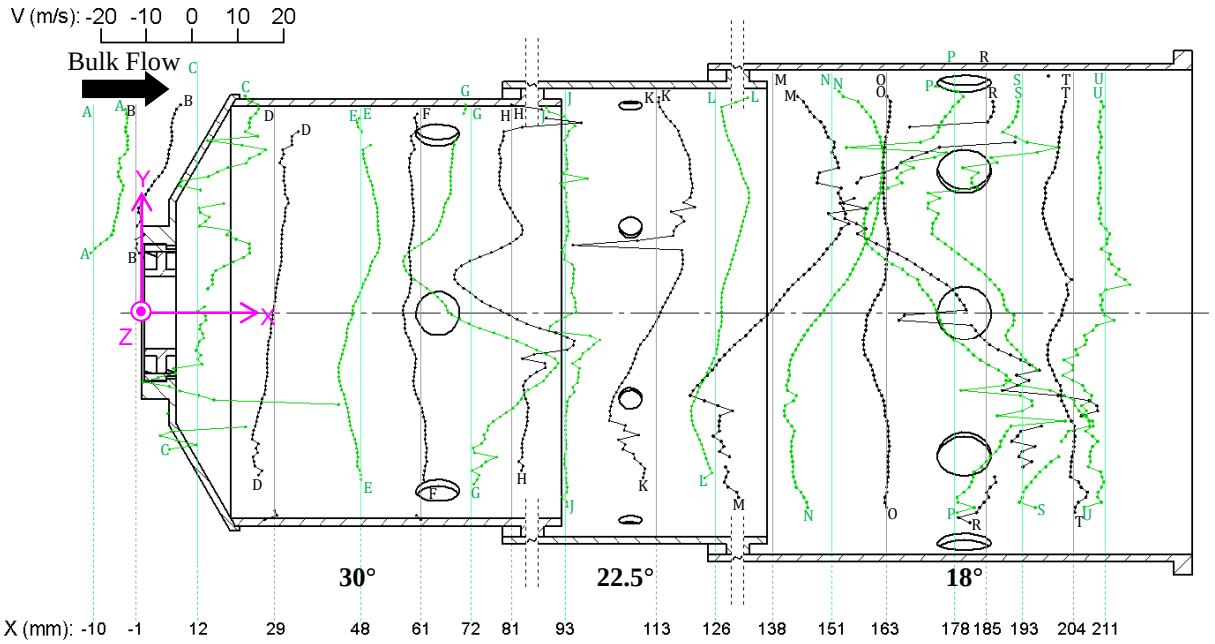

Figure 13: In between with the holes at $\dot{m}_A$ = 0.09 kg/s: The radial velocity profiles at various positions of the respective zones.

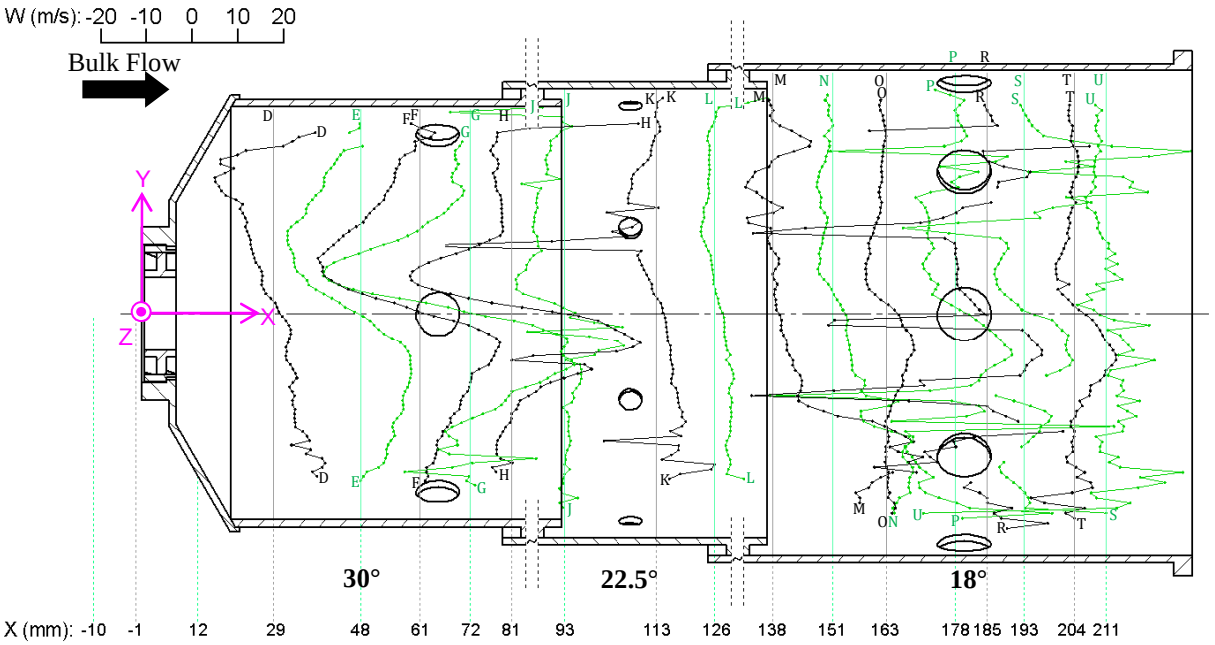

Figure 14: In between with the holes at $\dot{m}_A$ = 0.09 kg/s: The azimuthal velocity profiles at various positions of the respective zones.

The undulations and the penetration of the cold core through the hot gasses at some places could be explained by two features in the presented data.

Firstly, in Figure 6c, a photo of the flames during a reacting run is shown. The blue flames indicate regions of combustion reactions close to stochiometric while the orange flames represent off stochiometric combustion most likely in the rich regime. During the experiments the blue parts of the flames were "stationary" and did not seem to move or vary much in shape throughout the experiment. The orange flames, however, were constantly moving, wrapping around, growing and then shrinking. There did, however, seem to be a periodic pattern to the orange flame movement. On the left side of the combustor, from about 135° to 225°, a wedge of "no flame" can be seen. This missing flame was a constant feature and corresponds to part of the colder region between 135° and 260° seen in the outlet profile in Figure 6b. What can also be seen in the photograph are blue flame tongues that extended out of the primary zone and along the walls of the liner towards the outlet. These flame tongues corresponded (allowing for some swirl) in position to the hot undulations found around the hot regions. These corresponding undulations and tongues are shown in Figure 6b and c at the * a, b or c symbols. Secondly, these undulations could also be contributed to due to the axial velocity profile at the liner exit in line with the holes having a lower velocity magnitude than in between the holes which could then create further variations in the temperature at the walls.

Discussion

The PIV results showing the velocity fields and profiles can be used to ensure the flowfield inside the combustor is modelled correctly. This indirectly tests the applicability of the chosen turbulence model. The size and position of the recirculation regions can be used as an indicator for how well the turbulence model is performing in the simulation of both jets and swirling flow together. While the magnitude and shape of the tangential velocity profile is also a good tool to show how well the swirling flow was modelled. The atypical recirculation region in the dilution zone provides an additional test as to how well the CFD captures the real flow features present. The jet penetration can influence the rate of mixing in the combustor liner [12] thus the penetration depth of the jets is also an important characteristic to be well modelled using numerical techniques.

Overall, the main difference between the lower flow rate experiments [6] and the current velocity field is the velocity magnitude, especially in the region of the jets. The main flow features have not shown significant variation.

Once the velocity field is modelled correctly, the thermal results can be used to evaluate, to some degree, the accuracy of the combustion modelling used in CFD simulations on the same combustor.

The velocities measured both with and without combustion in the exhaust section can be used to evaluate the expected changes in the velocity field due to the addition of the combustion model.

Summary

The three-component velocity vector field was measured, using a stereoscopic PIV system, inside a transparent generic can-type gas turbine combustor. The PIV data was captured on planes in line with and in between the holes of each of the three zones of the combustor.

The main flow features such as the recirculation zones and jets were captured. An unexpected recirculation zone was observed in the dilution zone. The departure of the flow from the recirculation regions to join the bulk flow in the dilution zone was also shown which seems like it may be a critical feature that could explain some features measured during reacting tests.

For further comparison, the velocity profiles both with and without combustion in the exhaust were measured. These provide a means to compare the runs before and after combustion is modelled.

Further the temperature was measured on the outlet plane of the combustor liner for comparison to CFD simulations that would include combustion. In order to show the influence of the combustion on the velocities the velocity profile in the exhaust was measured using a Pitot tube both with and without combustion.

This data can be used effectively as a test case, both non-reacting and reacting combustor flow, for CFD due to the presence of all the flow features of the combustor as well as data showing the influence of the combustion on the velocity as well as thermal data for direct comparison.

Acknowledgements

This document is the result of a research effort funded by the Defence Research and Development Board, in terms of Armscor order KT521897.

References

[1] Vakil, S.S., Thole, K.A., "Flow and Thermal Field Measurements in a Combustor Simulator Relevant to a Gas Turbine Aeroengine", *Journal of Engineering for Gas Turbines and Power*, vol. 127, pp. 257-267, April 2005.

[2] Archer, S., Gupta, A.K., "Confinement Effects on Flow and Combustion under Fuel Lean Conditions", *Proceedings of IMECE04 2004 ASME International Mechanical Engineering Congress and Exposition*, Anaheim, California, USA, 13 - 20 November 2004.

[3] Mandai, S., Nishida, H., "Application of Turbulent Reacting Flow Analysis for Gas Turbine Combustor Development", *JSME International Journal*, vol. 47, no. No. 1, 2004, Series B.

[4] Janus, B., Dreizler, A., Janicka, J., "Flow Field and Structure of Swirl Stabilized Non-Premixed Natural Gas Flames at Elevated Pressure", *Proceedings of ASME Turbo Expo 2004 Power for Land, Sea and Air June 14-17 2004*, Vienna, Austria, June 2004.

[5] Li, G., Gutmark, E.J., "Boundary Condition Effects on Nonreacting and Reacting Flows in a Multiswirl Combustor", *AIAA Journal*, vol. 44, no. No. 3, pp. 444-456, March 2006.

[6] Meyers, B.C., Snedden, G.C., Meyer, J.P., Roos, T.H., Mahmood, G.I., "Three-Dimensional Particle Image Velocimetry in a Generic Can-Type Gas Turbine Combustor", *Proceedings of the IXX International Symposium on Air Breathing Engines (ISABE)*, Montreal, Canada, 7-11 September 2009, ISABE-2009-1108.

[7] Carl, M., Behrendt, T., Fleing, C., Frodermann, M., Heinze, J., Hassa, C., Meier, U., Wolff-Gassmann, D., Hohmann, S., Zarzalis, N., "Experimental and Numerical Investigation of a Planar Combustor Sector at Realistic Operating Conditions", *Journal of Engineering for Gas Turbine and Power*, vol. 123, pp. 810-816, October 2001.

[8] TSI Incorporated, "Insight™ 3G v 7.2.2.0", 2004.

[9] Tecplot Incorporated, "Tecplot v 10.0-6-012", 1988.

[10] Kline, S.J., McClintock, F.A., "Describing Uncertainties in Single-Sample Experiments", *Mechanical Engineering*, vol. 75, pp. 3-8, January 1953.

[11] Li, G., Gutmark, E.J., "Geometry Effects on the Flow Field and the Spectral Characteristics of a Triple Annular Swirler", *Proceedings of ASME Turbo Expo 2003 Power for Land, Sea and Air June 16-19 2003*, Atlanta, GGeorgia, USA, June 2003, GT2003-38799.

[12] Lefebvre, A.H., *Gas Turbine Combustion*, Hemisphere Publishing Corporation, United States of America, 1983.